Journal of Solid Mechanics Vol. 7, No. 2 (2015) pp. 191-203

Upper Bound Analysis of Tube Extrusion Process Through Rotating Conical Dies with Large Mandrel Radius

H. Haghighat *, M. M. Mahdavi

Mechanical Engineering Department, Razi University, Kermanshah, Iran

Received 6 March 2015; accepted 5 May 2015

ABSTRACT

In this paper, an upper bound approach is used to analyze the tube extrusion process through rotating conical dies with large mandrel radius. The material under deformation in the die and inside the container is divided to four deformation zones. A velocity field for each deformation zone is developed to evaluate the internal powers and the powers dissipated on all frictional and velocity discontinuity surfaces. By minimization of the total power with respect to the slippage parameter between tube and the die and equating it with the required external power, the extrusion pressure is determined. The corresponding results for rotating conical dies are also determined by using the finite element code, ABAQUS. The analytical results show a good coincidence with the results by the finite element method with a slight overestimation. Finally, the effects of various process parameters such as mandrel radius, friction factor, etc., upon the relative extrusion pressure are studied.

Keywords : Tube extrusion; Rotating conical die; Upper bound method.

1 INTRODUCTION

TUBE extrusion is a process in which tubes are manufactured by forcing a hollow billet through a die and the mandrel under high pressure. The mandrel is generally connected to the ram and moves with ram velocity. In extrusion process, die rotation reduces primary forming loads and improves the homogeneity of deformation [1]. To study the effects of the process parameters on the tube extrusion process through rotating conical dies, analytical solutions are preferred to the finite element method. Among various analytical methods of solutions, upper bound solutions are found by minimizing the total power formulated from a chosen kinematically admissible velocity field. Some attention has been focused on the upper bound analysis of axisymmetric extrusion (round to round) through rotating dies by assuming appropriate velocity fields. The so called KOBO type forming proposed by BOCHNIAK and KORBEL applied to extrusion of tubes and wires has demonstrated essential advantages with respect to monotonic forming processes [2-4]. Kim and Park studied the backward extrusion process with low die rotation to improve the problems of conventional backward extrusion process: the requirement of large forming machine, the difficulty in selecting the die material caused by high surface pressure, high cost of forming machine caused by improvement of noise and vibration, etc [5]. They used upper bound technique and FEM simulation. The results showed that the backward extrusion with die rotation is a very useful process because this process yields the homogeneous deformations and lower forming load. MA et al. analysed the process of forward rod extrusion

* Corresponding author. Tel.: +98 831 4274530; Fax: +98 831 4274542.
E-mail address: hhaghighat@razi.ac.ir (H. Haghighat).

through steadily rotating conical dies, theoretically and experimentally [6-7]. They provided required torque for rotating the die from an external source and also supposed that the angular velocity of the material inside the die changes with power relation with radius of each position in proportion to apex of virtual conic of the die. They inspected the effect of slippage factor and semi die angle in extrusion pressure and finally determined the optimum die angle. MACIEJEWSKI and MROZ analyzed the rod extrusion process through a flat die assisted by cyclic torsion, which was induced by a cyclically rotating die [8].

In this study, tube extrusion process with large mandrel radius through rotating conical dies, investigated analytically and numerically. The material under deformation is divided to four deformation zones. A velocity field for each deformation zone, considering slippage parameter between material and the die, is developed and the total power is calculated. By minimization of the total power with respect to the slippage parameter and equating it with the required external power, the extrusion pressure is determined. Based on developed analytical model, for a given process conditions and die angular velocity, the optimum die angle and the relative extrusion pressure are derived and they are compared with results of the FEM simulation data.

2 UPPER BOUND ANALYSIS

2.1 Geometric description of deformation zones

Schematic diagram of the tube extrusion process through a rotating conical die is shown in Fig. 1. In this figure, circular tube with initial outer radius R_o and inner radius R_m, respectively, is extruded through the conical die with semi-die angle α and its outer radius is reduced to R_f. As shown in this figure, a moving cylindrical shaped mandrel with radius R_m is attached to the punch. The material under deformation in the die and inside the container is divided to four deformation zones, I-IV shown in Fig. 1, and they are used in upper bound analysis. A spherical coordinate system (r,θ,φ) is used to describe the position of the two surfaces of velocity discontinuity and the velocity in deformation zones I and II. The origin of spherical coordinate system is located at point *O*. The material inside the container along the total length *L* is divided into two deformation zones, zones III and IV. Zone III is bounded by two velocity discontinuity surfaces S_2 and S_3, mandrel surface as well as the container surface. The material in this zone is twisted plastically. The billet in the remaining length $(L-l)$ is designated by zone IV. In this zone, the incoming material is assumed to flow horizontally as a rigid body with a velocity v_o. Zone IV is separated from zone III by a surface of velocity discontinuity S_3. This surface is located at radial distance r_o from the origin O', where distance OO' is equal to *L*. A cylindrical coordinate system (r,θ,y) is used to describe the velocity field in the deformation zones III and IV where the axial coordinate y is parallel to the extruding direction.

For the continuity of the normal component of velocity at the exit boundaries, surface S_1, must not be circular. The radial position of the exit boundary, $r_f(\theta)$ in Fig. 1, is given by:

$$r_f(\theta)=\frac{\sqrt{[(r_o\sin\theta+R_m)^2-R_m^2]\dfrac{R_f^2-R_m^2}{R_o^2-R_m^2}+R_m^2}-R_m}{\sin\theta} \tag{1}$$

$$r_1=\frac{R_o-R_m}{\sin\alpha} \tag{2}$$

where r_1 is value of $r_f(\theta)$ at $\theta=\alpha$. For simplicity $r_f(\theta)$ is abbreviated to r_f.

The mathematical equations for radial positions of the surface of velocity discontinuity S_2 is given by:

$$r_o=\frac{R_o-R_m}{\sin\alpha} \tag{3}$$

In addition to these surfaces, there are some frictional surfaces along mandrel surface, die wall and the container surface, $S_4 - S_9$.

2.2 Velocity fields in different zones

The first step in modelling and analysing a metal forming process by use of upper bound approach is to select a suitable velocity field for the material which is deforming plastically.

In zone I, the material moving in the axial direction and rotating along the die axis with constant angular velocity $\beta_1\omega_d$, where ω_d is the angular velocity of the die. The velocity field in spherical coordinate system (r,θ,φ) is:

$$\dot{U}_r = -v_f \cos\theta, \quad \dot{U}_\theta = v_f \sin\theta, \quad \dot{U}_\varphi = \beta_1\omega_d(R_m + r\sin\theta) \tag{4}$$

β_1 is the circumferential slippage parameter defined as the angular velocity ratio of material at exit of conical die to rotating die. Slippage parameter β_1 varies between 0 and 1, where the value of 1 implies that the extruded tube rotates at the same angular velocity as that of the die. The optimal value of β_1 can be determined by minimizing the extrusion pressure. v_f is the speed of the extruded tube and from the volume flow balance, we have

$$v_f = \frac{R_o^2 - R_m^2}{R_f^2 - R_m^2} v_o \tag{5}$$

In zone IV, material does not deform but moves as a rigid body in the axial direction with constant velocity of the punch v_o and we have

$$\dot{U}_r = 0, \quad \dot{U}_\theta = 0, \quad \dot{U}_y = v_o \tag{6}$$

For deformation zone II that is surrounded by two velocity discontinuity surfaces S_1 and S_2 and mandrel surface as well as the die surface. Assuming volume flow balance, the radial velocity $\dot{U}_r$ within the deformation zone II can be obtained. In Fig. 1, the volume flow of the material across the surfaces S_1 at the point (r_o,θ,φ) in the radial direction is:

$$dQ = -v_o \cos\theta(r_o d\theta)(R_m + r_o \sin\theta)d\varphi \tag{7}$$

The volume flow of the material in the radial direction at the point (r,θ,ϕ) in the deformation zone is:

$$dQ = U_r(rd\theta)(R_m + r\sin\theta)d\varphi \tag{8}$$

where angle θ is the angular position of a point in the deformation zone II. Equating Eqs. (7) and (8), the radial velocity component in zone II can be found.

$$\dot{U}_r = -v_o \frac{r_o}{r}\frac{R_m + r_o\sin\theta}{R_m + r\sin\theta}\cos\theta \tag{9}$$

The same circumferential component of velocity field was employed by Ma et al. to analyze rod extrusion process through rotating conical dies is extended here for tube extrusion process through rotating conical dies [7]. So the total velocity field is described by:

$$\dot{U}_r = -v_o \frac{r_o}{r}\frac{R_m + r_o\sin\theta}{R_m + r\sin\theta}\cos\theta \tag{10a}$$

$$\dot{U}_\theta = 0 \tag{10b}$$

$$\dot{U}_\varphi = \beta_1 \omega_d (R_m + r\sin\theta)(\frac{r_f}{r})^3 \tag{10c}$$

For deformation zone III, using cylindrical coordinate system (r,θ,y) in Fig. 1, it is assumed that

$$\dot{U}_y = v_o, \dot{U}_r = 0, \dot{U}_\theta = \beta_2(\Theta)\omega_d(R_m + r_o\sin\Theta)\frac{y - r_o(1-\cos\Theta)}{l} \tag{11}$$

with

$$\beta_2(\Theta) = \beta_1[\frac{r_f(\Theta)}{r_o}]^3 \tag{12}$$

where $\beta_2(\Theta)$ is the slippage parameter (angular velocity ratio of rod at entrance of conical die to rotating die) where angle γ is shown in Fig. 1 and varies between 0 and α.

Eqs. (10) and (11) satisfy the incompressibility condition as well as the boundary conditions, therefore they can be deemed as kinematically admissible fields.
With the velocity field, the strain rates in the deformation zone, internal power and the power consumed on the shear and frictional surfaces can be given in usual matter.

The strain rates in spherical coordinates are given by :

$$\dot{\varepsilon}_{rr} = \frac{\partial \dot{U}_r}{\partial r} \tag{13a}$$

$$\dot{\varepsilon}_{\theta\theta} = \frac{1}{r}\frac{\partial \dot{U}_\theta}{\partial \theta} + \frac{\dot{U}_r}{r} \tag{13b}$$

$$\dot{\varepsilon}_{\varphi\varphi} = \frac{1}{r + \frac{R_m}{\sin\theta}}(\frac{1}{\sin\theta}\frac{\partial \dot{U}_\varphi}{\partial \varphi} + \dot{U}_r + \dot{U}_\theta\cot\theta) \tag{13c}$$

$$\dot{\varepsilon}_{r\theta} = \frac{1}{2}(\frac{\partial \dot{U}_\theta}{\partial r} - \frac{\dot{U}_\theta}{r} + \frac{1}{r}\frac{\partial \dot{U}_r}{\partial \theta}) \tag{13d}$$

$$\dot{\varepsilon}_{\theta\varphi} = \frac{1}{2}(\frac{1}{r\sin\theta}\frac{\partial \dot{U}_\theta}{\partial \varphi} + \frac{1}{r}\frac{\partial \dot{U}_\varphi}{\partial \theta} - \frac{\dot{U}_\varphi}{r + \frac{R_m}{\sin\theta}}\cot\theta) \tag{13e}$$

$$\dot{\varepsilon}_{\varphi r} = \frac{1}{2}(\frac{\partial \dot{U}_\varphi}{\partial r} - \frac{\dot{U}_\varphi}{r + \frac{R_m}{\sin\theta}} + \frac{1}{r\sin\theta}\frac{\partial \dot{U}_r}{\partial \varphi}) \tag{13f}$$

where $\dot{\varepsilon}_{ij}$ (with $i \neq j$) is a shear strain rate component.

The strain rates components for deformation zone I are zero and the strain rates components for deformation zone II become

$$\dot{\varepsilon}_{rr} = v_o \frac{r_o}{r^2} \frac{R_m + r_o \sin\theta}{(R_m + r\sin\theta)^2} (R_m + 2r\sin\theta)\cos\theta \tag{14a}$$

$$\dot{\varepsilon}_{\theta\theta} = -v_o \frac{r_o}{r^2} \frac{R_m + r_o \sin\theta}{R_m + r\sin\theta} \cos\theta \tag{14b}$$

$$\dot{\varepsilon}_{\varphi\varphi} = -v_o \frac{r_o}{r} \frac{R_m + r_o \sin\theta}{(R_m + r\sin\theta)^2} \sin\theta\cos\theta \tag{14c}$$

$$\dot{\varepsilon}_{r\theta} = -v_o \frac{r_o}{2r^2} \frac{1}{(R_m + r\sin\theta)^2} \{(R_m + r\sin\theta)[r_o(\cos^2\theta - \sin^2\theta) - R_m \sin\theta] - r(R_m + r_o\sin\theta)\cos^2\theta\} \tag{14d}$$

$$\dot{\varepsilon}_{\theta\varphi} = \frac{3}{2} \frac{\beta_1 \omega_d r_f^2}{r^4} \frac{dr_f}{d\theta} (R_m + r\sin\theta) \tag{14e}$$

$$\dot{\varepsilon}_{\varphi r} = -\frac{3}{2} \beta_1 \omega_d (R_m + r\sin\theta) \frac{r_f^3}{r^4} \tag{14f}$$

The non-vanishing strain rate for the deformed tube inside container, zone III in Fig. 1, in cylindrical coordinate system (r, θ, y), is determined by:

$$\dot{\varepsilon}_{y\theta} = \frac{1}{2}\left(\frac{\partial \dot{U}_\theta}{\partial y} + \frac{1}{r}\frac{\partial \dot{U}_y}{\partial \theta}\right) = \frac{1}{2}\beta_2(\Theta)\omega_d \frac{R_m + r_o \sin\Theta}{l} \tag{15}$$

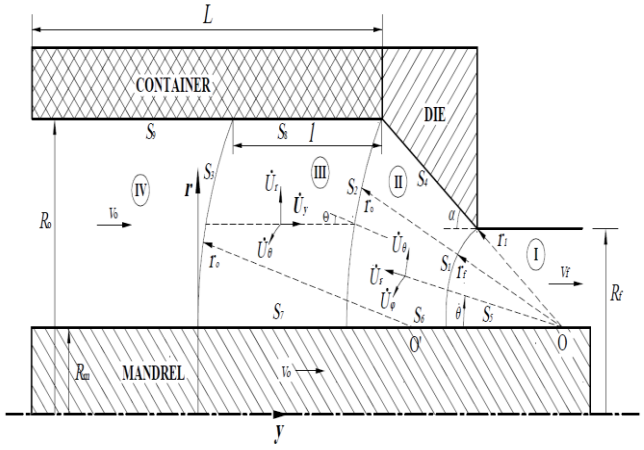

Fig.1
Schematic diagram of the tube extrusion process through a rotating conical die, geometric parameters and its deformation zones.

2.3 Internal power of plastic deformation

The internal power dissipated in the deformation zone is given by:

$$\dot{W}_i = \frac{2\sigma_0}{\sqrt{3}} \int_V \sqrt{\frac{1}{2}\dot{\varepsilon}_{ij}\dot{\varepsilon}_{ij}}\, dV \tag{16}$$

For deformation zone II, the differential volume is:

$$dV = 2\pi(R_m + r\sin\theta)r\,dr d\theta \tag{17}$$

The internal power of deformation in zone II becomes

$$\dot{W}_{i2} = \frac{4\pi}{\sqrt{3}}\sigma_0 \int_{r_f}^{r_o}\int_0^{\alpha}\sqrt{\frac{1}{2}\dot{\varepsilon}_{rr}^2 + \frac{1}{2}\dot{\varepsilon}_{\theta\theta}^2 + \frac{1}{2}\dot{\varepsilon}_{\varphi\varphi}^2 + \dot{\varepsilon}_{r\theta}^2 + \dot{\varepsilon}_{\theta\varphi}^2 + \dot{\varepsilon}_{\varphi r}^2}\;(R_m + r\sin\theta)r d\theta\, dr \tag{18}$$

For deformation zone III the differential volume is:

$$dV = (R_m + r_o\sin\Theta)r_o\cos\Theta d\Theta dy \tag{19}$$

The internal power of deformation in zone III is determined as:

$$\begin{aligned}\dot{W}_i &= \frac{4\pi}{\sqrt{3}}\sigma_\circ \int_0^{\alpha}\int_{\delta}^{l+\delta}(\frac{1}{2}\beta_2(\Theta)\omega_d\frac{R_m + r_o\sin\Theta}{l})(R_m + r_o\sin\Theta)r_o\cos\Theta d\Theta dy \\ &= \frac{2\pi}{\sqrt{3}}\sigma_\circ\omega_d\int_0^{\alpha}\beta_2(\Theta)(R_m + r_o\sin\Theta)^2 r_o\cos\Theta d\Theta\end{aligned} \tag{20}$$

where $\delta = r_o(1-\cos\Theta)$.

2.4 Shear power dissipation

The general equation for the power losses along a shear surface of velocity discontinuity in an upper bound model is:

$$\dot{W}_S = \frac{\sigma_0}{\sqrt{3}}\int_S |\Delta v|\, dS \tag{21}$$

Equation for the power losses along the shear surfaces of velocity discontinuity S_1 and S_2 can be given by:

$$\dot{W}_{S_1} = \frac{2\pi}{\sqrt{3}}\sigma_0 v_f\int_0^{\alpha} r_f[1+(\frac{1}{r_f}\frac{dr_f}{d\theta})^2](r_f\sin\theta + R_m)\sin\theta d\theta \tag{22}$$

$$\dot{W}_{S_2} = \frac{2\pi}{\sqrt{3}}\sigma_0 r_o\left[\frac{r_o}{2}(\alpha - \frac{\sin 2\alpha}{2}) + R_m(1-\cos\alpha)\right] \tag{23}$$

$$\dot{W}_{S_3} = 0 \tag{24}$$

2.5 Frictional power dissipation

The general equation for the frictional power losses along a surface with a constant friction factor *m* is:

$$\dot{W}_f = m\frac{\sigma_0}{\sqrt{3}}\int_{S_f} |\Delta v|\, dS \tag{25}$$

For the conical surface of the die, frictional surface S_4 , the magnitude of the velocity difference and the differential surface are

$$\Delta v_4 = \sqrt{\Delta v_r^2 + \Delta v_\varphi^2}, dS_4 = 2\pi(R_m + r\sin\alpha)dr \tag{26}$$

where

$$\Delta v_r = \dot{U}_r\big|_{\theta=\alpha} = v_o \frac{r_o}{r}\frac{R_m + r_o\sin\alpha}{R_m + r\sin\alpha}\cos\alpha \tag{27}$$

$$\Delta v_\varphi = (R_m + r\sin\alpha)\omega_d - \dot{U}_\varphi\big|_{\theta=\alpha} = (R_m + r\sin\alpha)\omega_d[1-\beta_1\frac{r_f^3(\alpha)}{r^3}] \tag{28}$$

Inserting Eqs. (27)-(28) into Eq. (26) and then placing into Eq. (25), gives the frictional power losses along the conical surface of the die as:

$$\dot{W}_{f4} = \frac{2\pi}{\sqrt{3}} m_d\sigma_0 \int_{r_1}^{r_o} \sqrt{[v_o\frac{r_o}{r}(R_m + r_o\sin\alpha)\cos\alpha]^2 + [(R_m + r\sin\alpha)^2\omega_d(1-\frac{\beta_1 r_f^3(\alpha)}{r^3})]^2}\, dr \tag{29}$$

where m_d is the constant friction factor between the material and the die.

For frictional surface S_5

$$\Delta v_5 = \sqrt{(v_f - v_o)^2 + (\beta_1\omega_d R_m)^2}, dS_5 = 2\pi R_m dr \tag{30}$$

$$\dot{W}_{f5} = \frac{2\pi}{\sqrt{3}} m_m R_m\sigma_0 r_f(0)\sqrt{(v_f - v_o)^2 + (\beta_1\omega_d R_m)^2} \tag{31}$$

For frictional surface S_6

$$\Delta v_6 = \sqrt{\Delta v_r^2 + \Delta v_\varphi^2}, dS_6 = 2\pi R_m dr \tag{32}$$

where

$$\Delta v_r = |\, v_o - v_o\frac{r_o}{r}\,| \tag{33}$$

and

$$\Delta v_\varphi = \dot{U}_\varphi at\ (\theta = 0) = \beta_1\omega_d R_m\frac{r_f^3(0)}{r^3} \tag{34}$$

The frictional power losses along frictional surface S_6 can be determined by:

$$\dot{W}_{f6} = \frac{2\pi}{\sqrt{3}} m_m\sigma_0 R_m \int_{r_f(0)}^{r_o} \sqrt{(v_o(1-\frac{r_o}{r}))^2 + [\beta_1\omega_d R_m\frac{r_f^3(0)}{r^3}]^2}\, dr \tag{35}$$

where m_m is the constant friction factor between the material and the mandrel.

For frictional surface S_7:

$$\Delta v_7 = \dot{U}_\theta \big|_{\theta=0} = \beta_2(0)\omega_d R_m \frac{y}{l}, dS_7 = 2\pi R_m dy \tag{36}$$

The frictional power losses along the surface S_7 can be given by:

$$\dot{W}_{f7} = \frac{\pi}{\sqrt{3}} m_m \sigma_0 R_m^2 \beta_2(0)\omega_d l \tag{37}$$

The velocity discontinuity on surface S_8 and its area become

$$\Delta v_8 = \sqrt{v_o^2 + \dot{U}_\theta^2}, dS_8 = 2\pi R_o dy \tag{38}$$

The frictional power losses along surface S_8 can be given by:

$$\dot{W}_{f8} = \frac{2\pi}{\sqrt{3}} m_c \sigma_0 R_o \int_{r_o(1-\cos\alpha)}^{l+r_o(1-\cos\alpha)} \sqrt{v_o^2 + [\beta_2(\alpha)\omega_d R_o \frac{y - r_o(1-\cos\alpha)}{l}]^2}\, dy \tag{39}$$

where m_c is the constant friction factor between the material and the container.

Finally, the frictional power loss along surface S_9 is:

$$\dot{W}_{f9} = \frac{2\pi}{\sqrt{3}} m_c \sigma_0 R_o v_o (L - l) \tag{40}$$

where L is length of tube in the container.

2.6 Twist moments

In addition to the power applied by the punch, a twist moment M_d is supplied by the rotating die. To determine this moment, it is assumed that the friction vector mk on a point at the die-material interface is opposite of resultant velocity [7]. The rotational component of the resultant velocity ΔV_4 is $\Delta V_{\varphi 4}$ and it is determined by:

$$\Delta v_{\varphi 4} = (R_m + r\sin\alpha)\omega_d - \dot{U}_\varphi \big|_{\theta=\alpha} = (R_m + r\sin\alpha)\omega_d (1 - \beta_1 \frac{r_f^3(\alpha)}{r^3}) \tag{41}$$

The angle γ_4 between ΔV_4 and $\Delta V_{\varphi 4}$ is calculated by:

$$\cos\gamma_4 = \frac{\Delta V_{\varphi 4}}{\Delta V_4} \tag{42}$$

The twist moment inserted by die rotation can therefore be derived by:

$$M_d = \frac{2\pi}{\sqrt{3}} m_d \sigma_0 \int_{r_1}^{r_o} \cos\gamma_4 (R_m + r\sin\alpha)^2 dr \tag{43}$$

The twist moment generates in the mandrel surfaces, S_5, S_6 and S_7 can be derived from

$$M_5' = \frac{2\pi}{\sqrt{3}}\sigma_0 m_m R_m^2 \int_0^{r_f(0)} \cos\gamma_5 dr, \cos\gamma_5 = \frac{\Delta v_{5\varphi}}{\Delta v_5} \tag{44}$$

$$M_6' = \frac{2\pi}{\sqrt{3}}\sigma_0 m_m R_m^2 \int_{r_f(0)}^{r_o} \cos\gamma_6 dr, \cos\gamma_6 = \frac{\Delta v_{6\varphi}}{\Delta v_6} \tag{45}$$

$$M_7' = \frac{2\pi}{\sqrt{3}}\sigma_0 m_m R_m^2 \int_0^{l} \cos\gamma_7 dy, \cos\gamma_7 = \frac{\Delta v_{7\theta}}{\Delta v_7} \tag{46}$$

The twist moment within the container is given as:

$$M_8' = \frac{2\pi}{\sqrt{3}}\sigma_0 m_c R_o^2 \int_{r_o(1-\cos\alpha)}^{l+r_o(1-\cos\alpha)} \cos\gamma_8 dy, \cos\gamma_8 = \frac{\Delta v_{8\theta}}{\Delta v_8} \tag{47}$$

As the balance among twisting moments must be maintained, the moment applied by the rotary die is balanced with summing up the moments caused by the circumferential frictions in the container and on the mandrel. The balance of the couples gives

$$M_d = M_5' + M_6' + M_7' + M_8' \tag{48}$$

The twisting length *l* can be determined by satisfying Eq. (48) with a given β_1 .

2.7 Total power

Based on the upper bound model, the total power needed for a tube extrusion process can be obtained by summing the internal powers and the powers dissipated on all frictional and velocity discontinuity surfaces and by ignoring the overlapping between zones II and III as:

$$J^* = \dot{W}_{i2} + \dot{W}_{i3} + \dot{W}_{S1} + \dot{W}_{S2} + \dot{W}_{f4} + \dot{W}_{f5} + \dot{W}_{f6} + \dot{W}_{f7} + \dot{W}_{f8} + \dot{W}_{f9} \tag{49}$$

The total external power is given by:

$$J^* = \sigma_{ave}\pi(R_o^2 - R_m^2)v_o + M_d\omega_d \tag{50}$$

Therefore, the total upper bound solution for relative extrusion pressure is given by:

$$\frac{\sigma_{ave}}{\sigma_0} = \frac{\dot{W}_{i2} + \dot{W}_{i3} + \dot{W}_{S1} + \dot{W}_{S2} + \dot{W}_{f4} + \dot{W}_{f5} + \dot{W}_{f6} + \dot{W}_{f7} + \dot{W}_{f8} + \dot{W}_{f9} - M_d\dot{\omega}_d}{\pi(R_o^2 - R_m^2)v_o\sigma_0} \tag{51}$$

All integrals that are presented in the power terms are evaluated by numerical integration. The total power in equation above is a function of semi-cone angle. The optimum semi-cone angle that minimizes the total power can be determined numerically.

3 RESULTS AND DISCUSSION

To make a comparison with the developed model, the tube extrusion process is simulated by using the finite element code, ABAQUS. Friction factors $m_c = 0.2, m_d = 0.2$ and $m_m = 0.2$, radii $R_o = 10mm$, $R_f = 8.19mm$, $R_m = 2mm$,

extruding speed $v_o = 1 mm/\sec$ are adopted during the analytical solution and the FEM simulation.

A three-dimensional model is used for FEM analyses. The billet model is meshed with C3D8R elements. Punch, mandrel, container and die are assumed as rigid bodies, since they are not meshed. However, sufficiently fine meshing is essential in material, which undergoes plastic deformation. The die model is able to rotate along its axis of symmetry and the punch model is loaded by specifying displacement in the axial direction. Also, container model is fixed by applying displacement constraint on its nodes. Fig. 2(a) illustrates the mesh used to analyze the deformation in extrusion of the tube through conical die with $\alpha = 20^\circ$ and $\omega = 0.5 rad/\sec$. Deformed model of the tube is shown in Fig. 2(b). As it is expected, the material is twisted in the die and inside the container.

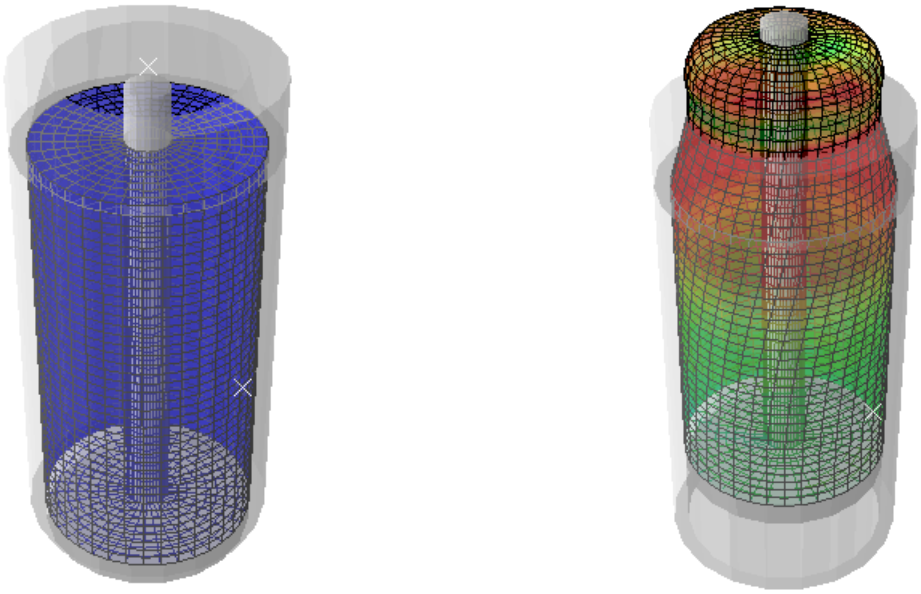

(a) (b)

Fig.2
(a) The finite element mesh, (b) The deformed mesh of tube in extrusion process through rotating conical die.

In Fig. 3, the relative extrusion pressure for different angular velocity of the die, obtained from the upper bound solution is compared with the FEM simulation results. The results show a good agreement between the upper bound data and the FEM results.

This figure also shows that with increasing of the angular velocity of the die the relative extrusion pressure is decreased but this reduction saturates at a high die angular velocity.

In Fig. 4, the relative extrusion pressure for different semi-die angle obtained from the upper bound solution is compared with the FEM simulation results. The results show a good agreement between the upper bound data and the FEM results. As it is expected, there is an optimum die angle in which the extrusion pressure is minimized.

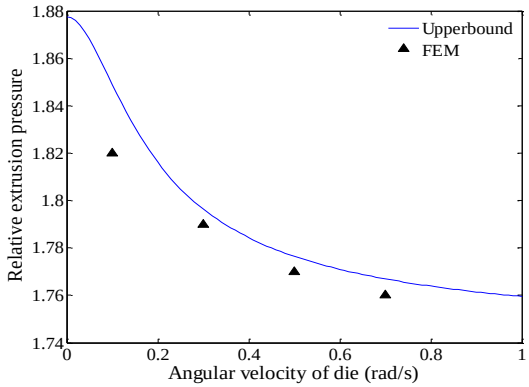

Fig.3
Comparison of analytical relative extrusion pressure with FEM data for different angular velocity of the die.
$v_o = 1 mm/\sec, R_o = 10 mm, R_f = 8.19 mm, R_m = 2 mm, \alpha = 20^\circ,$
$m_d = 0.2, m_c = 0.2, m_m = 0.2$

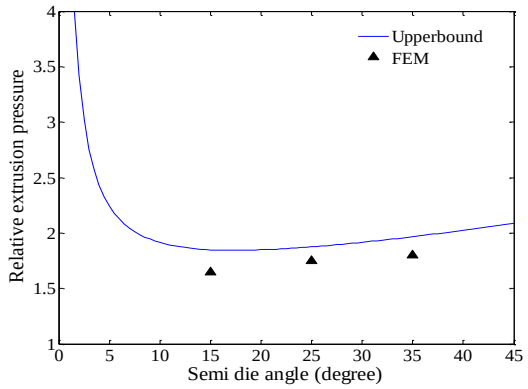

Fig.4
Comparison of analytical relative extrusion pressure with FEM data for different semi-die angles.
$v_o = 1mm/\sec, R_o = 10mm, R_f = 8.19mm, R_m = 2mm,$
$\omega = 0.1rad/\sec, m_d = 0.2, m_c = 0.2, m_m = 0.2$

The effect of mandrel radius on the relative extrusion pressure is illustrated in Fig. 5. It is seen that the extrusion pressure is increased by increasing the mandrel radius.

The effect of angular velocity on the relative extrusion pressure for different values of die friction factors is shown in Fig. 6. It is observed that the extrusion pressure is decreased by increasing the die angular velocity and decreasing the die friction factor but this reduction saturates at a high die angular velocity.

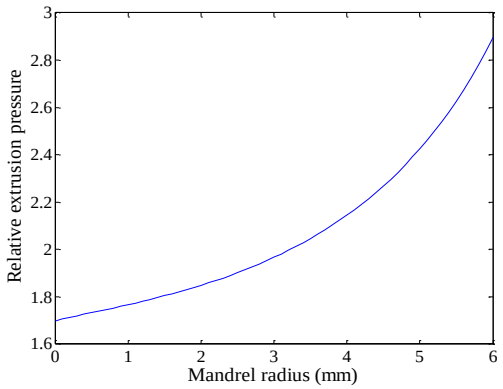

Fig.5
Effect of mandrel radius on the relative extrusion pressure for
$v_o = 1mm/\sec, R_o = 10mm, R_f = 8.19mm, \omega = 0.1rad/\sec$
$m_d = 0.2, m_c = 0.2, m_m = 0.2$

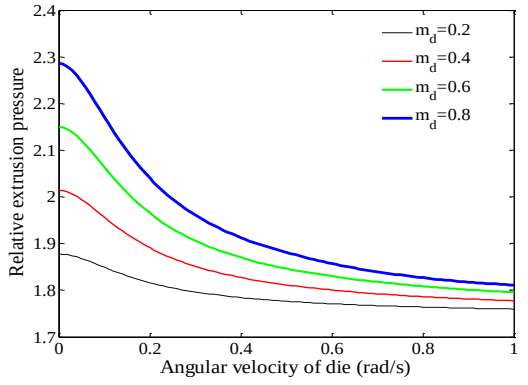

Fig.6
Effect of angular velocity of the die on the relative extrusion pressure for different friction factors of die.
$v_o = 1mm/\sec, R_o = 10mm, R_f = 8.19mm, R_m = 2mm,$
$\omega = 0.1rad/\sec, m_c = 0.2, m_m = 0.2$

The effect of die angle on the relative extrusion pressure for different values of die friction factors is shown in Fig. 7. As it is expected, for a given value of die friction factor, there is an optimal die angle, which minimizes the extrusion pressure and the optimum die angle increases when friction factor of die increases. This figure also shows that an increase in the friction factor of die tends to increase the extrusion pressure.

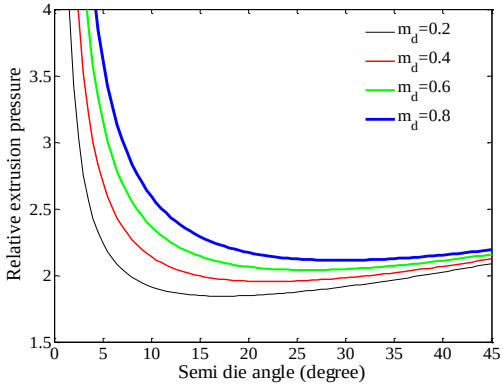

Fig.7
Effect of semi-die angle on the relative extrusion pressure for different friction factors of die.
$v_o = 1mm/\sec, R_o = 10mm, R_f = 8.19mm, R_m = 2mm,$
$\omega = 0.1rad/\sec, m_c = 0.2, m_m = 0.2$

The effect of angular velocity on the relative extrusion pressure for different values of the tube entrance speed is shown in Fig. 8. It is observed that the extrusion pressure is decreased by decreasing the die angular velocity and decreasing the entrance speed but this reduction is low at high entrance speeds.

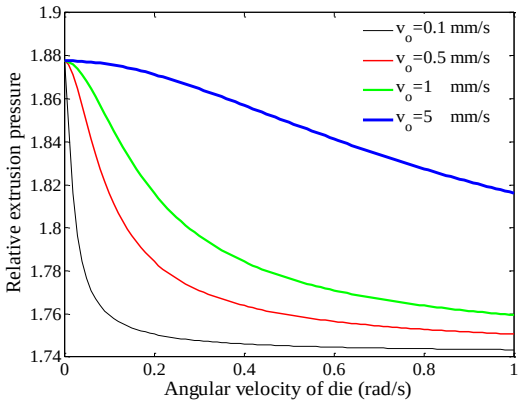

Fig.8
Effect of angular velocity of the die on the reduction of extrusion pressure for different extruding speeds.
$R_o = 10mm, R_f = 8.19mm, R_m = 2mm, \alpha = 20^\circ, m_d = 0.2,$
$m_c = 0.2, m_m = 0.2$

5 CONCLUSIONS

In this research, an upper bound model for analysis of the tube extrusion process through rotating conical dies was developed and it was concluded that

1. The analytical results by the analytical method showed a good coincidence with the results by the FEM with a slight overestimation.
2. With increasing of the angular velocity of the die, the relative extrusion pressure was decreased but this reduction saturates at a high die angular velocity.
3. The relative extrusion pressure was increased by increasing the mandrel radius.
4. The relative extrusion pressure was decreased by decreasing the die friction factor but this reduction saturates at a high die angular velocity.
5. For a given value of die friction factor, there was an optimal die angle, which minimizes the extrusion pressure and the optimum die angle increases when friction factor of die increases.
6. Twisting length of the material inside the container decreases when friction factor of die increases.
7. The relative extrusion pressure is decreased by decreasing the entrance speed but this reduction is low at high entrance speeds.

REFERENCES

[1] Ma X., Barnett M., 2005, An upper bound analysis of forward extrusion through rotating dies, *In Proceedings of the 8th ESAFORM Conference on Material Forming*, Bucharest, Romania.

[2] Bochniak W., Korbel A., 1999, Extrusion of CuZn39Pb2 alloy by the KOBO method, *Engineering Transactions* **47**: 351-367.

[3] Bochniak W., Korbel A., 2000, Plastic flow of aluminum extruded, under complex conditions, *Matererials Science and Technology* **16**: 664-674.

[4] Bochniak W., Korbel A., 2003, KOBO-type forming: forging of metals under complex conditions of the process, *Journal of Materials Processing Technology* **134**: 120-134.

[5] Kim Y.H., Park J.H., 2003, Upper bound analysis of torsional backward extrusion process, *Journal of Materials Processing Technology* **143-144**: 735-740.

[6] Ma X., Barnett M., Kim Y. H., 2004, Forward extrusion through steadily rotating conical dies, Part I: experiments, *International Journal of Mechanical Sciences* **46**: 449- 464.

[7] Ma X., Barnett M., Kim Y. H., 2004, Forward extrusion through steadily rotating conical dies, Part II: theoretical analysis, *International Journal of Mechanical Sciences* **46**: 465-489.

[8] Maciejewski J., Mroz Z., 2008, An upper-bound analysis of axisymmetric extrusion assisted by cyclic torsion, *Journal of Materials Processing Technology* **206**: 333-344.